J. Fluid Mech. (2006), *vol.* 550, *pp.* 27–42.
doi:10.1017/S0022112005007743 Printed in the United Kingdom

Hydromagnetic Taylor–Couette flow at very small aspect ratio

By ANTHONY J. YOUD AND CARLO F. BARENGHI

School of Mathematics, University of Newcastle, Newcastle upon Tyne, NE1 7RU, UK

(Received 1 January 2005 and in revised form 5 July 2005)

The work of Benjamin, Mullin, Pfister and others on the non-uniqueness of solutions of the Navier–Stokes equation in Couette flow at small aspect ratio has revealed the existence of 'anomalous' 1-cell modes. A natural question to ask is whether these 'anomalous' modes are robust enough to survive the application of a body force, such as an externally applied magnetic field. We find that the answer is positive, although, with increasing magnetic field, steady 2-cell flows are generally more stable than 1-cell states. We also show that new time-dependent flows are easy to excite at relatively low Reynolds numbers compared to the case without a magnetic field, and we present two such flows.

1. Introduction

Our concern is the motion of an incompressible conducting viscous fluid confined between two rotating concentric cylinders in the presence of an axial magnetic field. Without the magnetic field, this problem (hydrodynamic Couette flow) is one of the most studied in fluid dynamics. The problem of the stability of Couette flow in the presence of a magnetic field has been almost forgotten after the pioneering work of Chandrasekhar (1961) and Donnelly & Ozima (1962), but is now undergoing a renaissance. What motivates most of the current interest in this and related configurations (e.g. spherical) are the astrophysical implications, such as the magnetorotational instability (Willis & Barenghi 2002*a*; Goodman & Ji 2002; Rüdiger, Schultz & Shalybkov 2003; Sisan *et al.* 2004) and dynamo action (Dobler, Shukurov & Brandenburg 2002; Willis & Barenghi 2002*b*). The most immediate application of our paper is however another. The work of Benjamin (1978*a*,*b*), Benjamin & Mullin (1981), Cliffe (1983), Pfister *et al.* (1988), Cliffe, Kobine & Mullin (1992), Mullin, Toya & Tavener (2002), Furukawa *et al.* (2002) and Lopez & Marques (2003) has highlighted the non-uniqueness of the Navier–Stokes equations and the importance of using small aspect ratios in the Couette configuration to reduce the multiplicity of solutions available. This approach led to the discovery of the so-called 'anomalous' modes induced by end effects. These modes have a direction of rotation of one or both of the end cells which is apparently counter-intuitive. Near the endwalls, the centrifugal forces are weakened by the stationary boundaries, and one would expect flows toward the inner cylinder (inflow). On the contrary, anomalous modes appear to have an outflow near the endwalls. Closer examination reveals the existence of small vortices in all four corners but they are very much weaker than the larger vortices. From the point of view of bifurcation theory, the main feature of anomalous modes is that they are disconnected from the primary flow (with the exception that, as the ratio of the height of the cylinders to the gap width becomes very small, the

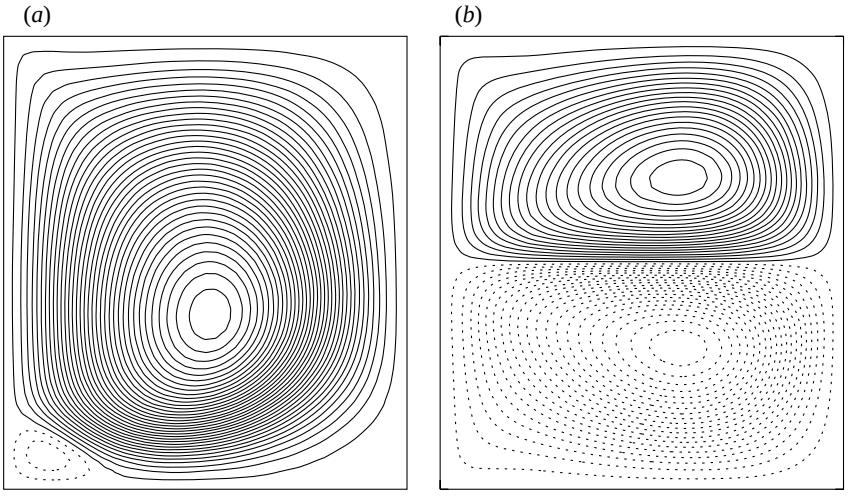

FIGURE 1. Computed contours of the stream function for (*a*) the 1-cell ($\mathscr{C}_1$) and (*b*) 2-cell ($\mathscr{C}_2$) modes at $\Gamma = 1.2$, $\eta = 0.5$, $Re = 400$. Solid contours represent vortices rotating counter-clockwise; dashed contours represent vortices rotating clockwise. The inner cylinder is on the left and the outer cylinder on the right.

anomalous 1-cell state is connected to the primary 2-cell solution and can be realized by a smooth increase in the Reynolds number).

Figure 1 illustrates steady 1-cell and 2-cell modes. In (*a*) the flow is asymmetric about the midplane and the axial velocity is non-zero there, whereas in (*b*) the flow is symmetric about the midplane and the axial velocity is zero.

The natural question which we ask is: what is the effect of a body force on the interaction between 1- and 2-cell modes? A convenient choice of body force is the Lorentz force. To answer this question we thus impose an axial magnetic field, generalizing the work of Mullin and collaborators from the hydrodynamic to the hydromagnetic case. For simplicity we restrict our study to aspect ratios of order unity.

2. Governing equations and boundary conditions

We consider an incompressible viscous fluid of constant kinematic viscosity ν, magnetic diffusivity λ, magnetic permeability μ_0, and density ρ, contained in the gap between two coaxial concentric cylinders of radii R_1 and R_2, and height, h. We assume that the outer cylinder is at rest while the inner cylinder rotates with prescribed angular frequency, Ω.

A magnetic field, $\boldsymbol{B}_0 = B_0\hat{\boldsymbol{z}}$ is applied in the axial direction where we assume cylindrical coordinates (r, θ, z), and we make our equations dimensionless using $\delta = R_2 - R_1$ as the length scale, δ^2/ν as the time scale, ν/δ as the velocity scale and B_0 as the magnetic scale. The dimensionless parameters in the problem are the radius ratio $\eta = R_1/R_2$, the inner-cylinder Reynolds number $Re = R_1\Omega\delta/\nu$, the aspect ratio $\Gamma = h/\delta$, the Chandrasekhar number $Q = B_0^2\sigma\delta^2/(\rho\nu)$ (where $\sigma = 1/(\lambda\mu_0)$) and the magnetic Prandtl number $P_m = \nu/\lambda$.

Laboratory liquid metals have very small magnetic Prandtl numbers, for example, $P_m \sim O(10^{-5})$ and $O(10^{-7})$ for liquid sodium and gallium respectively. In the small Prandtl number limit we expect that $\boldsymbol{B} \sim O(P_m)$ and $\boldsymbol{u} \sim O(1)$ where $\boldsymbol{u}$ is the fluid

velocity. Letting $\boldsymbol{B} = P_m \boldsymbol{b}$ we have the following hydromagnetic equations:

$$\partial_t \boldsymbol{u} + (\boldsymbol{u}\cdot\nabla)\,\boldsymbol{u} = -\nabla p + \nabla^2 \boldsymbol{u} + Q\,(\nabla \wedge \boldsymbol{b}) \wedge \hat{\boldsymbol{z}}, \tag{2.1a}$$

$$\nabla \cdot \boldsymbol{u} = 0, \tag{2.1b}$$

$$\nabla^2 \boldsymbol{b} = -\nabla \wedge (\boldsymbol{u} \wedge \hat{\boldsymbol{z}})\,, \tag{2.1c}$$

$$\nabla \cdot \boldsymbol{b} = 0, \tag{2.1d}$$

where p is the pressure. We assume that all fields are axisymmetric, in agreement with experimental findings at low and moderate Reynolds numbers (the exception being an experiment by Pfister, Schulz & Lensch (1991) at high Reynolds numbers mentioned in § 4). We then solve equations (2.1) by a finite-difference method using the stream function–vorticity formulation (which corresponds to azimuthal magnetic field and current). Typically we use $N_r = 80$ radial grid-points and $N_z = N_r \Gamma$ axial grid-points with time steps Δt of the order of 10^{-4} or 10^{-5}. The time-integration combines Crank–Nicolson and Adams–Bashforth methods, which are second-order accurate in the time step; the spatial discretization is based on second-order-accurate finite differences. The Poisson equations for the stream function and azimuthal magnetic field and current are solved using parallel ScaLAPACK (Blackford *et al.* 1997) linear algebra routines. Since the matrices involved do not depend on time, an LU factorization is performed before the time integration begins. This factorization is then used in a call to a solver routine at each time step. The use of a time-stepping code allows us to examine transients as steady states are approached and also to determine the structure of time-dependent solutions in the (r, z)-plane. Steady-state solutions are computed by monitoring the linear growth rate of the radial and/or axial velocities at the point $\mathscr{P} = ((R_1 + R_2)/2, h/2)$. The growth rate of the radial velocity is given by

$$\sigma_r = \frac{1}{\Delta t} \ln \left| \frac{u_r^{n+1}}{u_r^n} \right|, \tag{2.2}$$

where n is the time index corresponding to the time $t = n\Delta t$; and similarly for the growth rate of the axial velocity σ_z. For a symmetric 2-cell flow the axial velocity at $\mathscr{P}$ is zero. In a time-stepping scheme such as ours the axial velocity decays quickly to zero after an initial transient and the growth rate of the axial velocity σ_z is negative. In this case we monitor the growth rate of the radial velocity σ_r at the same point and use the following criterion: a steady state has been reached when $|\sigma_r| < 10^{-8}$. For an asymmetric 1-cell flow the axial velocity at $\mathscr{P}$ is non-zero and as the time-stepping proceeds $|u_z|$ increases. In this case we require that both $|\sigma_r| < 10^{-8}$ and $|\sigma_z| < 10^{-8}$ at $\mathscr{P}$ for a steady state to have been reached.

The boundary conditions for the stream function and vorticity can be derived from the usual no-slip conditions, so $u_r = u_z = 0$ at $r = R_1,\ R_2$, $u_\theta = Re$ at $r = R_1$, and $u_\theta = 0$ at $r = R_2$. Additionally, we require no-slip boundary conditions at the top and bottom endwalls, so $u_r = u_\theta = u_z = 0$ at $z = 0,\ h$. The boundary conditions for the magnetic field depend on the conductivity of the cylinders as discussed in Roberts (1964). Hereafter, we assume perfectly conducting cylinders and so the boundary conditions for the azimuthal magnetic field and current, $\boldsymbol{J}$, are $(1/r)B_\theta + \partial_r B_\theta = 0$ and $J_\theta = 0$ at $r = R_1,\ R_2$, and $\partial_z B_\theta = 0$ and $J_\theta = 0$ at $z = 0,\ h$. The Appendix gives a more complete description of the boundary conditions. An important point to consider is the effect of the discontinuity which arises between the rotating inner cylinder and the fixed endwalls where the azimuthal velocity increases from 0 to Re. This discontinuity is present in any experiment where a small gap must be left between the inner cylinder and the end walls to prevent a temperature gradient building up which would occur

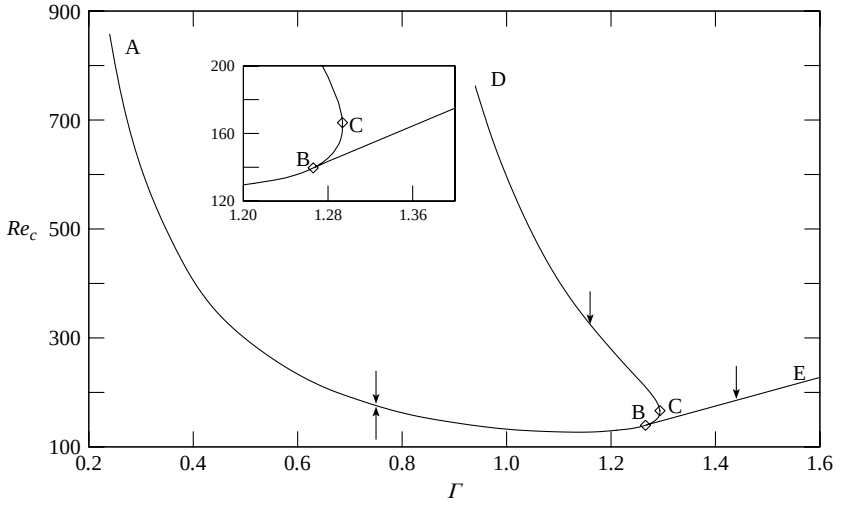

FIGURE 2. Critical Reynolds number Re_c versus aspect ratio Γ for the transition between the 1- and 2-cell flows without a magnetic field, $Q = 0$, for $\eta = 0.5$. The arrows denote whether the boundaries can be found by a quasi-static increase (↑) or decrease (↓) of the Reynolds number. The inset is an enlargement of the hysteresis region.

if the boundaries were allowed to meet. The exact form of the relevant boundary condition to model this would be very difficult to determine and so many numerical calculations use a small parameter $\epsilon \ll 1$ which allows the azimuthal velocity to vary smoothly between the boundary values along the endwalls. The calculations in the previously cited works have used mesh refinement in the corners but it is generally found that provided the mesh size is small enough in the corners the disturbance caused by the discontinuity is local to the corners and does not extend significantly into the fluid. Lücke *et al.* (1984) remarked that no anomalies could be found within a distance of 0.2 mm of the corners of their experimental apparatus with a gap width of $\delta = 1.126$ cm. Nevertheless, we tested our code on a finer mesh by increasing the number of radial grid points from 80 to 160. We calculated the critical Reynolds numbers at $\Gamma = 0.25$ on the curve AB in figure 2, and at $\Gamma = 0.97$ on the curve CD, where the greatest inaccuracies lie in our code. The critical Reynolds numbers are altered by 0.1% with the increase in the number of mesh points. Therefore, in our numerical code we do not implement mesh refinement or give any special treatment to the discontinuity in the corners.

3. Results: steady flows

The purely hydrodynamic case ($Q = 0$) was first studied experimentally by Benjamin & Mullin (1981) and then numerically by Cliffe (1983) at radius ratio $\eta = 0.615$. At the same time as Cliffe's work Lücke *et al.* (1984) numerically and experimentally studied the problem, although they only considered one aspect ratio $\Gamma = 1.05$ at radius ratio $\eta = 0.5066$. The problem was later also studied numerically and experimentally by Pfister *et al.* (1988) at radius ratio $\eta = 0.5$ who also determined time-dependent boundaries. The papers by Benjamin & Mullin (1981), Cliffe (1983), and Pfister *et al.* (1988) all produced bifurcation diagrams similar to figure 2. The figure shows our numerical results for the interaction between the 1-cell and 2-cell modes at $\eta = 0.5$, which agree with those of Pfister *et al.* (1988) to graphical accuracy. It is unfortunate

that in the literature critical Reynolds numbers are usually displayed as graphs, but are rarely tabulated. Cliffe (1983) gives actual numerical values of critical Reynolds numbers at three different aspect ratios $\Gamma = 0.67$, 1.00, and 1.187 ($\Gamma = 0.67$ and 1.187 were where the greatest inaccuracies lay in his finite-element code) but his radius ratio is different to ours so a direct comparison is not possible. Instead we compare the critical values obtained by our code to graphically estimated values of Pfister *et al.* (1988). At $\Gamma = 0.67$ (on AB) our critical Reynolds number is 202.8, at $\Gamma = 1.00$ (on AB) it is 132.8, and at $\Gamma = 1.187$ (on CD) it is 292.6. The corresponding (graphically estimated $\sim \pm 7\%$) critical values of Pfister *et al.* (1988) are 200, 132, and 295. Our results differ from those of Pfister *et al.* (1988) by approximately 1.4%, 0.6%, and 0.8% at the three values of Γ considered.

Mullin *et al.* (2002) further explored the parameter space by considering larger Reynolds numbers and other radius ratios and found bifurcations of 1- and 2-cell flows (at $\eta = 0.5$) for $\Gamma \lesssim 0.7$. (A graphical estimate ($\sim \pm 2\%$) of their critical Reynolds number at $\Gamma = 0.67$ is $Re_c = 205$) which differs from that of Pfister *et al.* (1988) by 2.5% and from ours by 1.1%. Time-dependent flows also exist in this region $\Gamma \lesssim 0.7$. The curve ABCD corresponds to a path of symmetry-breaking bifurcation points. As the Reynolds number is increased quasi-statically across AB, the symmetric 2-cell state loses stability and the asymmetric 1-cell state sets in. Any further increase in the Reynolds number simply increases the amplitude of the 1-cell solution. The same instability from 2-cell flow (obtained by suddenly starting the inner cylinder at a value above CD) to 1-cell flow is found as the Reynolds number is decreased quasi-statically across CD; if the Reynolds number is further decreased the 2-cell state regains stability as the curve AB is crossed. In the small range of Γ between B and C there is hysteresis between the 1-cell and 2-cell modes. Finally, the curve BE corresponds to a path of limit points of the 1-cell flow. In this range of Γ, the 2-cell flow no longer loses stability to the 1-cell flow as the Reynolds number is increased quasi-statically. The 1-cell flow is now disconnected and can only be obtained by a trick, such as a jump of the aspect ratio from inside the region ABCD to the region outside, holding the Reynolds number above the critical value; BE is thus a stability boundary only for decreasing Reynolds number. Schematic bifurcation diagrams of these three cases can be seen in figure 3. The hysteresis region may be extremely sensitive to imperfections in an experimental apparatus and also to inaccuracies in a numerical code. Pfister *et al.* (1988) explicitly state the range of Γ for which the hysteresis is present and they determined it to be $1.267 \leqslant \Gamma \leqslant 1.304$; using our numerical code we have found the phenomenon to exist for $1.267 \leqslant \Gamma \leqslant 1.294$. The agreement is excellent.

The methods used to determine paths of steady symmetry-breaking bifurcations depend on whether the boundaries can be found with both a quasi-static increase and decrease of the Reynolds number (e.g. the path AB) or whether the boundary can be found in only one direction (e.g. the paths CD and BE). Sufficiently close to the critical Reynolds number for the onset of asymmetry σ_z at $\mathscr{P}$ is approximately constant. If $\sigma_z > 0$ then $|u_z|$ is increasing and an asymmetric state sets in; if $\sigma_z < 0$ then $|u_z|$ is decreasing and a symmetric state sets in. The boundary AB was found in the following way: the Reynolds number is set to a value just below critical and once σ_z is constant (i.e. σ_z varies by less than 10^{-8} between successive time-steps) the sign of σ_z is checked. The Reynolds number is then automatically stepped in arbitrarily small increments until a change of sign in σ_z is detected. Once this change of sign occurs a bisection method is employed to determine the critical Reynolds number. At the critical Reynolds number $|\sigma_z|$ is found to be less than 10^{-6}. Finding the boundary

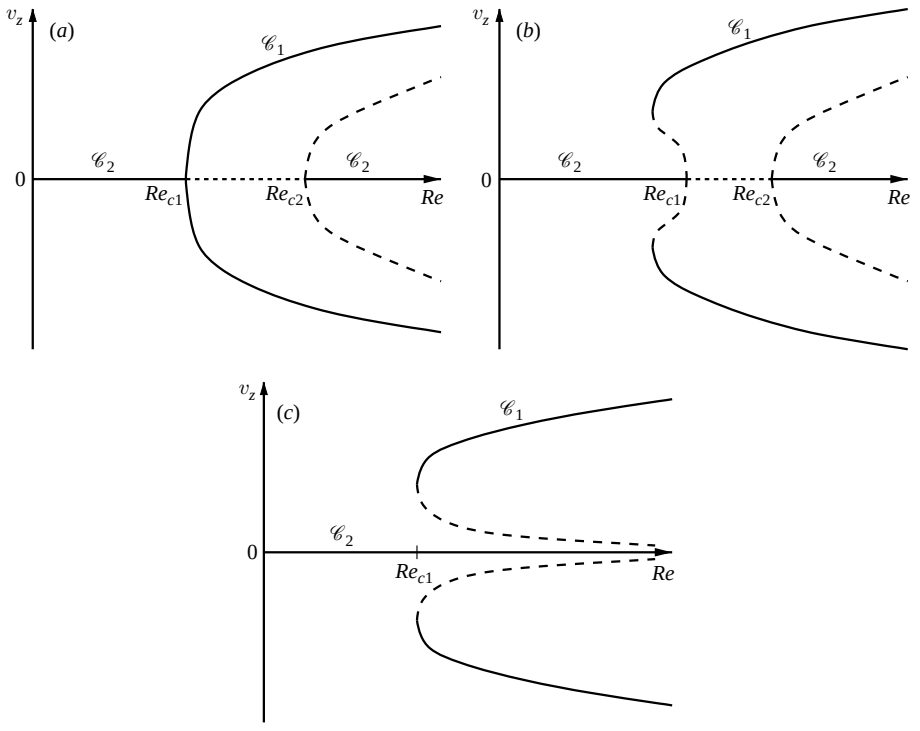

FIGURE 3. Schematic bifurcation diagrams for the interaction between the 1- and 2-cell states after Pfister *et al.* (1988). The vertical axis shows the amplitude of the axial velocity v_z in the middle of the gap at $z = h/2$ which distinguishes between symmetric and asymmetric flows. The Reynolds number is on the horizontal axis. Re_{c1} and Re_{c2} are the critical Reynolds numbers for the onset of the 1-cell and 2-cell flows respectively. $\mathscr{C}_1$ denotes (stable) 1-cell branches; $\mathscr{C}_2$ denotes (stable) 2-cell branches. In (*a*) the 1-cell solution branch is connected (the curve AB in figure 2); in (*b*) there is hysteresis between the 1- and 2-cell flows (BC); in (*c*) the 1-cell solution branch is disconnected (CE). Stable branches are shown as solid lines, unstable branches as dashed lines.

CD is a little more difficult since it can be found only by a quasi-static decrease of the Reynolds number after a sudden start of the cylinder to a Reynolds number above the critical value. The Reynolds number is automatically decreased in small steps until σ_z switches sign from negative to positive (indicating a transition from a symmetric to an asymmetric state). It is then no longer possible to increase the Reynolds number again, since CD can only be found by a decrease in the Reynolds number. To overcome this difficulty the Reynolds number is instantaneously set to zero and then to a value above critical after the axial velocity has decayed sufficiently. In this way it is possible to carry out the bisection method using the two Reynolds numbers between which a change of sign of σ_z occurs, approaching the critical value only from above the boundary CD. At the critical Reynolds number $|\sigma_z|$ is again found to be less than 10^{-6}. The path BE and the hysteresis region are found in similar ways with further minor modifications.

Figure 4 shows the same bifurcation diagram as in figure 2 but now including various strengths of applied magnetic field ($Q \neq 0$).

The general trend is that, by increasing the magnetic field, the instability to 1-cell flows is pushed to higher Reynolds numbers, so 2-cell flows are more likely. In a qualitative sense, this is consistent with the findings of Chandrasekhar (1961) that,

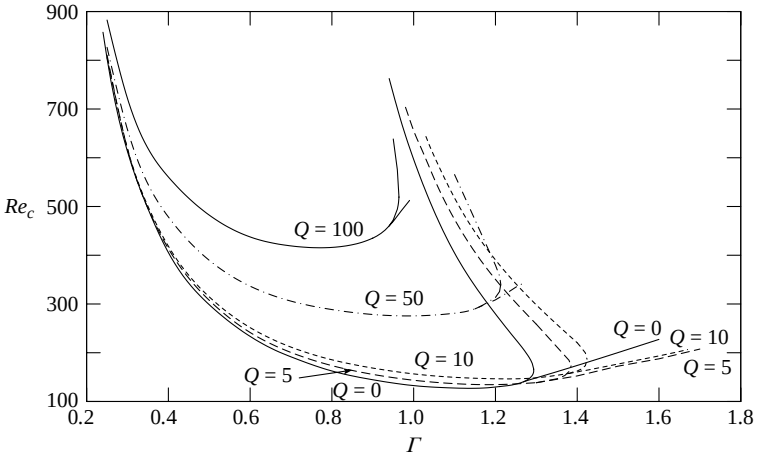

FIGURE 4. Critical Reynolds number Re_c versus aspect ratio Γ for the transition between the 1- and 2-cell flows (as figure 2) in the presence of various applied magnetic fields, Q.

for $\Gamma \to \infty$ and $Q \lesssim 100$, the characteristic axial wavelength decreases. Schulz, Pfister & Tavener (2003) considered the effect of outer cylinder rotation on the transition between the 1- and 2-cell states and found that symmetric 2-cell flows were stabilized by co-rotation of the cylinders with the stabilizing effect being greater the larger the rotation rate of the outer cylinder; in fact for a certain value of the outer cylinder Reynolds number (at $\Gamma = 1$) the 2-cell state remained stable for all rotation rates of the inner cylinder examined. We have found a similar effect with the application of a magnetic field; for the same aspect ratio ($\Gamma = 1$) there is a critical Q at which the 1-cell state is no longer realizable. This can be seen in figure 4 where, with $Q = 100$, the 1-cell state no longer exists for a quasi-static increase of the Reynolds number.

This stabilization of the 2-cell flow is less pronounced as the aspect ratio is decreased and all curves seem to tend to an asymptote at approximately $\Gamma = 0.2$. It was shown by Mullin *et al.* (2002) at various radius ratios that there is a critical value of Γ below which the 1-cell flow no longer exists, and the flow is symmetric and unique, at least for not too large Reynolds numbers. The left-hand side of figure 4 shows that the application of a magnetic field does not alter Mullin's critical aspect ratio.

There is another critical aspect ratio, Γ_c, (corresponding to the point C in figure 2) at which the 1-cell flow is no longer realizable by a quasi-static increase of the Reynolds number across AB or decrease across CD. Figure 5 shows Γ_c versus Q. Apparently, Γ_c increases with increasing Q for $Q \lesssim 10$ but then for $Q \gtrsim 10$ it decreases with increasing Q.

Figures 6 and 7 show contour plots of various fields in the presence of an applied magnetic field, $Q = 100$. The aspect ratio of $\Gamma = 0.97$ is chosen in such a way so as to allow both the 1- and 2-cell flows to exist at the same Reynolds number, $Re = 500$, ensuring a fairer comparison, with only the route taken through parameter space differing in each case. It is apparent from both sets of figures that the cells are compressed toward the inner cylinder. This is in contrast to the case of no magnetic field, $Q = 0$, as in figure 1 (albeit at slightly different aspect ratio and Reynolds number) where the cells are much more centrally located. Goodman & Ji (2002) show similar contour plots of the stream function and azimuthal magnetic field (as well as the flux function and azimuthal velocity perturbation) with both perfectly

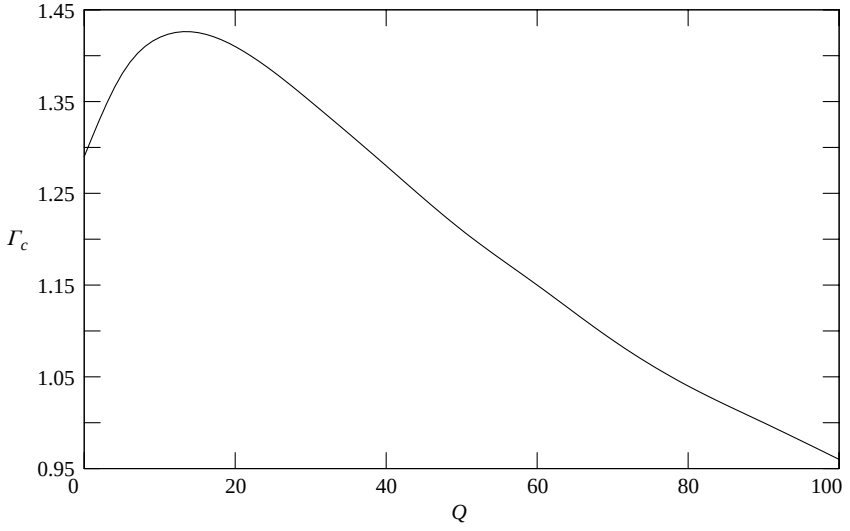

FIGURE 5. Critical aspect ratio Γ_c versus Q (the point at which the 1-cell flow is no longer realizable by a quasi-static increase of Re across the curve AB or decrease across the curve CD).

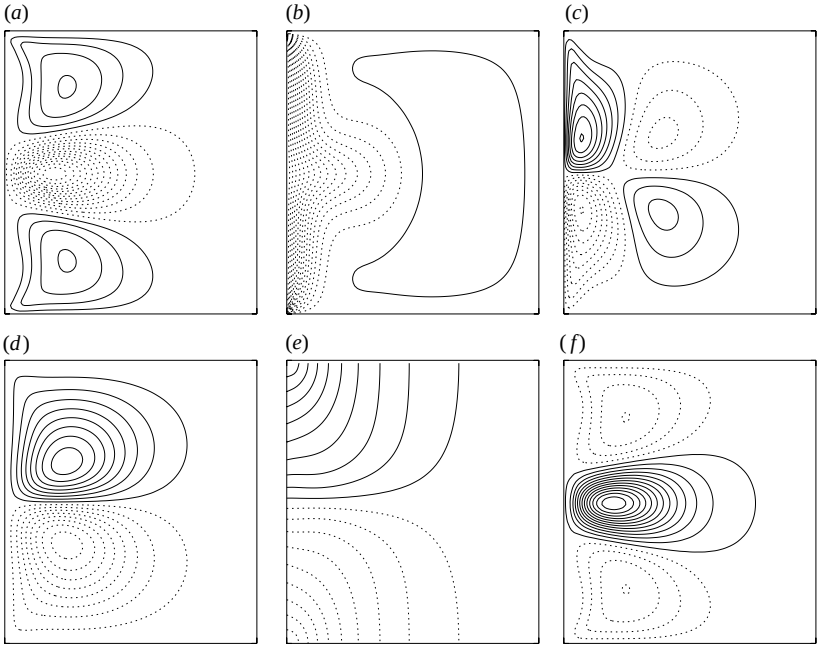

FIGURE 6. Computed contours of various fields for a 2-cell flow for $Q = 100$, $Re = 500$, $\Gamma = 0.97$. Inner cylinder on the left. (*a*) Radial velocity, u_r, (*b*) azimuthal velocity, u_θ (including the underlying circular Couette flow), (*c*) axial velocity, u_z, (*d*) stream function, ψ, (*e*) azimuthal magnetic field, B_θ, (*f*) azimuthal current, J_θ.

conducting and insulating boundaries for the infinite cylinder case. From their plots (with conducting boundaries) it is also evident that the cells are compressed toward the inner cylinder under the influence of a magnetic field.

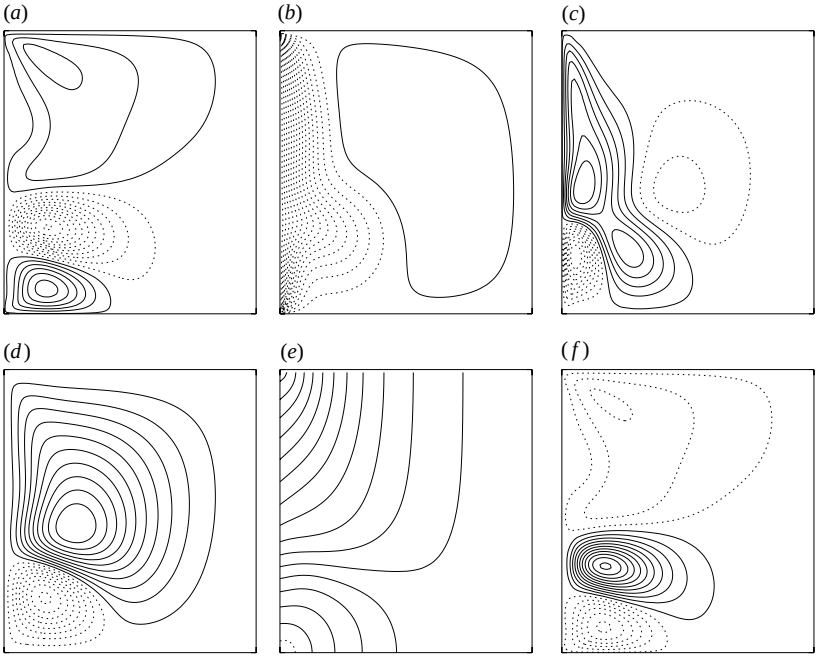

FIGURE 7. Contour plots as in figure 6 with the same parameters but now for a 1-cell flow.

4. Results: time-dependent flows

So far we have been concerned only with steady flows. Time-dependent 1- and 2-cell states at aspect ratios up to $\Gamma \approx 0.5$ have been described in the literature. Pfister *et al.* (1988) discovered axisymmetric oscillations for $\Gamma \gtrsim 0.35$; this time-dependence disappeared for $\Gamma \gtrsim 0.55$. Furukawa *et al.* (2002) confirmed the existence of time-dependence in this region. Lopez & Marques (2003) extended the study to include non-axisymmetric motion for a fixed aspect ratio of $\Gamma = 0.5$ and found interesting dynamics including double Hopf bifurcations, Neimark–Sacker bifurcations to a modulated rotating wave, and saddle-node-infinite-period bifurcations. These time-dependent solutions for $\Gamma \lesssim 0.5$ are not included in figure 2 for clarity. In this paper we concentrate on what happens to the right-hand side of figure 2, where we have discovered that the magnetic field induces time-dependence at relatively small Reynolds numbers.

Figure 8 shows the critical Reynolds number, Re_{td}, for the onset of time-dependent flow versus aspect ratio at various strengths of magnetic field. For $Q = 0$, the 1-cell mode realized by a quasi-static increase in the Reynolds number across AB in figure 2 undergoes a Hopf bifurcation to the unsteady state across the curve XY. The transition between steady 1-cell flow and time-dependent flow takes place in both directions (either increasing Re or decreasing it) for aspect ratios less than Γ_c; for aspect ratios larger than this, the transition boundary can only be found by a quasi-static decrease of the Reynolds number. Γ_c is represented as a vertical bar on each of the curves in the figure. The Hopf bifurcation for $Q = 0$ is in a regime where the Reynolds number is so high (above 1000) that our assumption of axisymmetry may be invalid. In fact, Pfister *et al.* (1991) experimentally determined a 1-cell state which undergoes a Hopf bifurcation for a range of aspect ratios and Reynolds numbers similar to those we report. The oscillation of this state is interrupted as the Reynolds number is

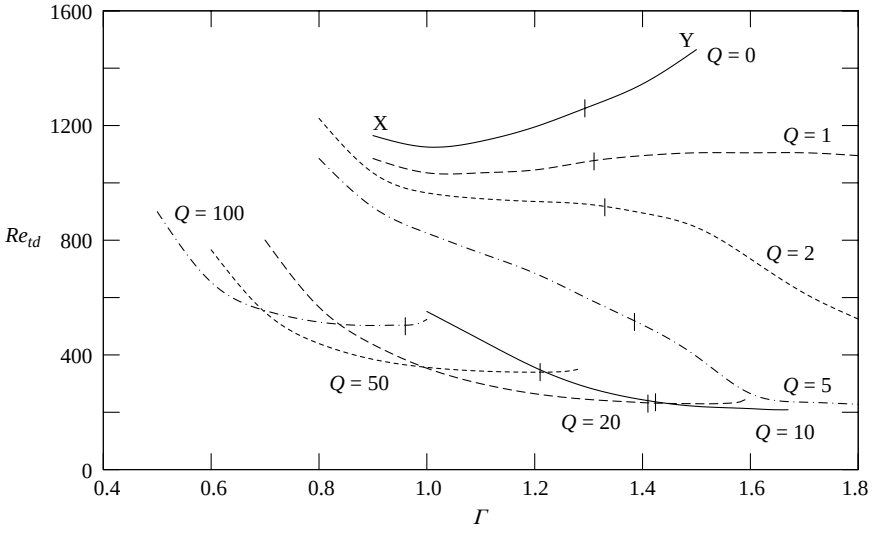

FIGURE 8. Critical Reynolds number Re_{td} versus aspect ratio Γ for the transition to time-dependent motion at various strengths of magnetic field, Q. To the left of the vertical bar on each curve (which corresponds to the aspect ratio of the point C on figure 2) the time-dependent boundary can be realized by a quasi-static increase or decrease of the Reynolds number; to the right it can only be found by a quasi-static decrease.

steadily increased and a stationary state sets in, which exists for a range of Reynolds numbers before the oscillatory state is resumed. They found that this unsteady mode is non-axisymmetric and has azimuthal wavenumber $m = 2$ or 3.

Note that, for $Q = 0$, the critical Reynolds number Re_{td} for the onset of time-dependent flow increases with increasing Γ. The most important finding is that, if Q is increased from $Q = 0$, the curve XY moves down to regions of much smaller Reynolds number, as shown in figure 8. If Q becomes larger than about 15, the 2-cell flow becomes more stable and Re_{td} increases, delaying the onset of time-dependence to higher Reynolds numbers (but still much less than for $Q = 0$).

We find that the path of limit points, BE of the 1-cell state merges with XY at the point Y (which, for $Q \geqslant 5$, corresponds to the rightmost point of each curve in figure 8). As the Reynolds number is decreased quasi-statically across XY, to the left of Y the time-dependent flow disappears and the 1-cell state regains stability; a further decrease of the Reynolds number across BE causes the appearance of the 2-cell state. To the immediate right of Y the 1-cell flow no longer exists as the Reynolds number is decreased and instead the 2-cell flow immediately regains stability.

We also find that there is an intersection of the curves CD and XY which, for smaller Q, occurs at high Reynolds numbers. As the strength of the magnetic field is increased further this intersection tends to the point C. The bifurcations that the system undergoes are slightly different to the left and to the right of this point. This is shown schematically in figure 9. In (*a*), to the left of the intersection, the 2-cell state (created by a sudden start of the inner cylinder to a value higher than the transition) first loses stability to the time-dependent state as the Reynolds number is decreased across CD, before this flow then loses stability to the 1-cell flow as the Reynolds number is further decreased across XY. However, in (*b*), to the right of the intersection, the 2-cell state does not lose stability to the time-dependent state as

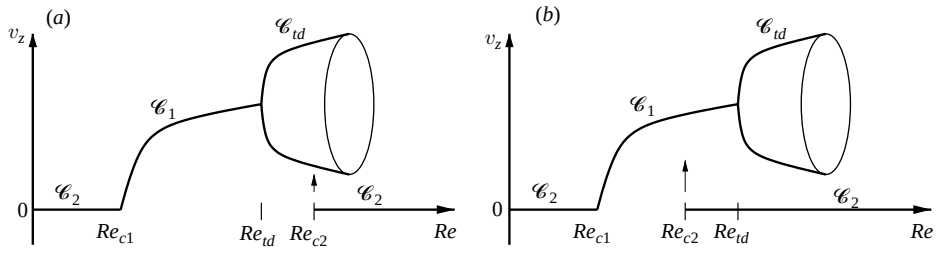

FIGURE 9. Schematic bifurcation diagrams (*a*) to the left and (*b*) to the right of the intersection point of curves CD and XY. The arrows denote the critical Reynolds number at which the 2-cell flow loses stability to (*a*) the time-dependent flow and (*b*) the 1-cell flow.

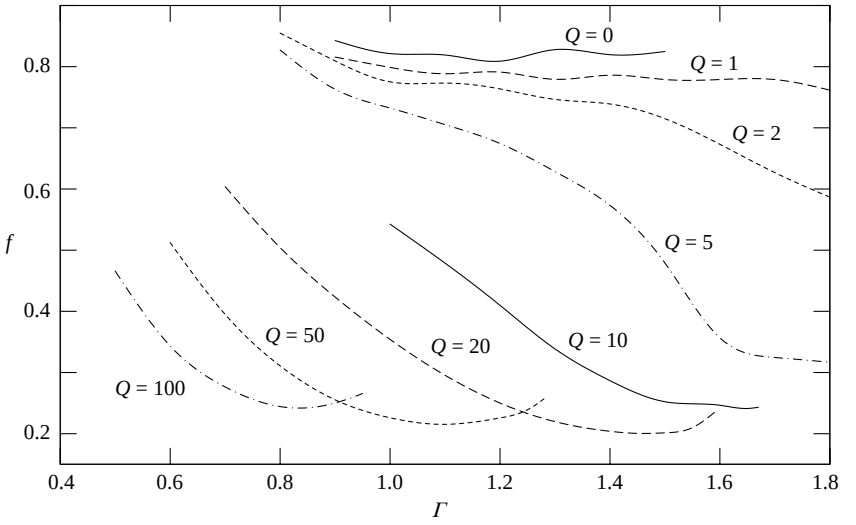

FIGURE 10. Frequency f of the oscillations at the onset of axisymmetric time-dependence versus aspect ratio Γ at various strengths of magnetic field Q. f is non-dimensionalized with respect to the inner-cylinder angular frequency, Ω. The relation between f and ω, the frequency which has been non-dimensionalized with respect to the diffusion time δ^2/ν, is $\omega = Re(1-\eta)f/\eta$.

the Reynolds number is decreased across XY, and instead loses stability to the 1-cell state as the Reynolds number is decreased across CD.

Figure 10 shows the frequency f of the oscillations at the onset of time-dependence versus the aspect ratio Γ at various strengths of applied magnetic field Q. Here, f is non-dimensionalized with respect to the inner cylinder angular frequency, Ω.

Note that the curves of f versus Γ follow the same trend as the curves of Re_{td} versus Γ of figure 8: f is lower the higher Q is. All frequencies f which we have found are much higher (at least one order of magnitude higher) than values of f reported by Pfister *et al.* (1988) in the absence of a magnetic field.

The nature of these time-dependent flows is revealed by figure 11, which shows contour plots of the stream function at various times over one period for $Q = 10$. Initially, in (*a*), the flow has the familiar 1-cell structure with a large main vortex and a smaller vortex in the corner near to the inner cylinder. Then the large vortex is deformed slightly and a very weak third vortex begins to appear near the inner cylinder at the upper-left corner. As the third vortex travels down the inner cylinder

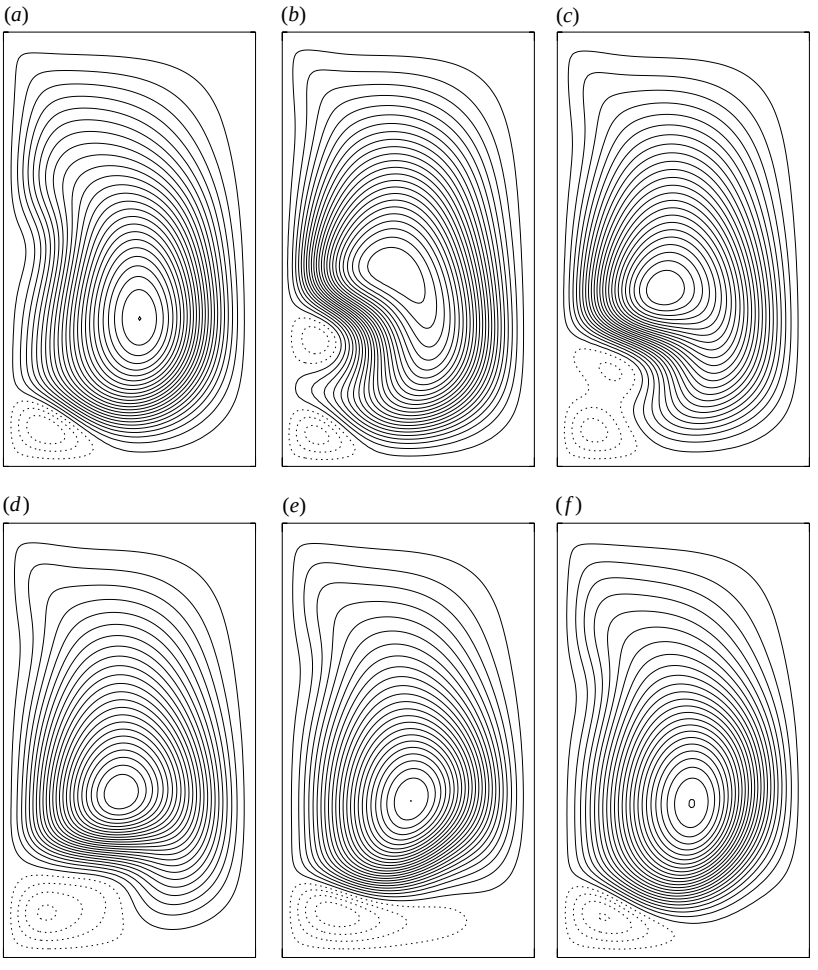

FIGURE 11. Snapshots of the stream function over one period for the time-dependent flow for $Q = 10$, $Re = 400$, and $\Gamma = 1.7$. Inner cylinder on the left, outer on the right. Solid contours represent vortices rotating counter-clockwise; dashed contours represent vortices rotating clockwise. (*a*) $t = 25.9857$, (*b*) $t = 25.9962$, (*c*) $t = 25.9998$, (*d*) $t = 26.0034$, (*e*) $t = 26.0091$, (*f*) $t = 26.0142$.

it becomes stronger as shown in (*b*). In (*c*) the third vortex begins to merge with the second vortex in the lower-left corner until a vortex roughly twice the size of the original second small vortex is produced in (*d*). In (*e*) this new vortex spreads across the gap towards the outer cylinder and splits in two in (*f*), before the process is repeated again. Although there is no direct evidence that this flow is the same as the one observed by Lensch (1988) and Pfister *et al.* (1991) the spatial-temporal dependence does bear a qualitative resemblance to their non-axisymmetric time-dependent flow; the main difference is that the third vortex which appears near the inner cylinder travels all the way around the first vortex.

We have also discovered the existence of a time-dependent 2-cell flow which exists for both $Q = 0$ and $Q \neq 0$. Contour snapshots of this flow can be seen in figure 12 for $Q = 10$, $Re = 700$, and $\Gamma = 1.3$. The effect is quite subtle and not as easy to see as the 1-cell time-dependence; the oscillation is caused by each cell, in turn, tilting and

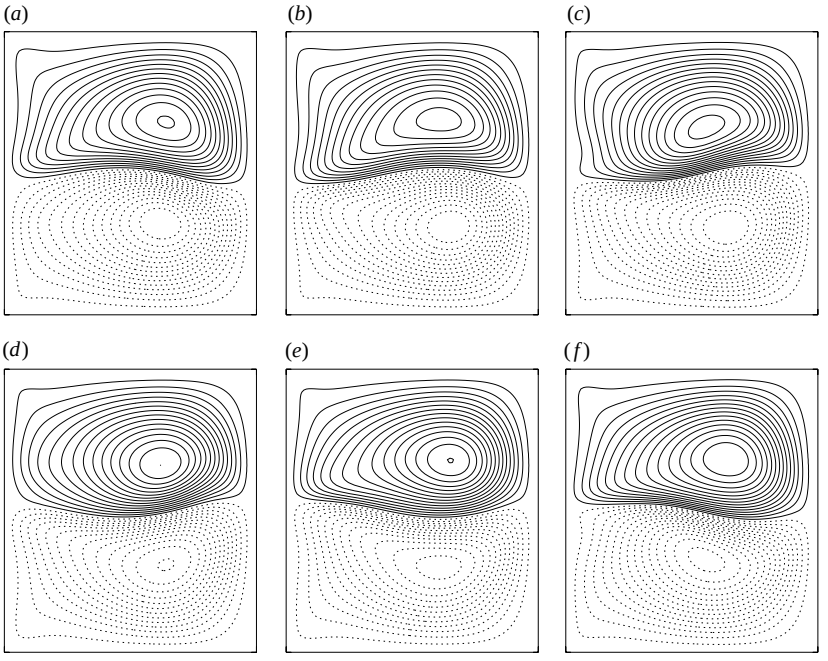

FIGURE 12. Snapshots of the stream function over one period for the time-dependent 2-cell flow for $Q = 10$, $Re = 700$, and $\Gamma = 1.3$. Inner cylinder on the left, outer on the right. Solid contours represent vortices rotating counter-clockwise; dashed contours represent vortices rotating clockwise. (*a*) $t = 4.0453$, (*b*) $t = 4.0477$, (*c*) $t = 4.0500$, (*d*) $t = 4.0524$, (*e*) $t = 4.0548$, (*f*) $t = 4.0572$.

growing larger across the midplane. Figures 13(*a*) and 13(*b*) show enlarged views of the right-hand side of the transition diagrams for $Q = 0$ and $Q = 10$. They show the interaction of the 1-cell and 2-cell steady flows, the 1-cell time-dependent flow (XY) and also the 2-cell time-dependent flow (ST). We found this flow by instantaneously setting the Reynolds number, from seed, to a value above the transition, and then decreasing the Reynolds number until a new flow structure emerged. For the case $Q = 0$, and for the aspect ratios considered, the time-dependent 2-cell flow has a critical Reynolds number below that of the time-dependent 1-cell flow. For $Q = 10$ the situation is reversed. For both $Q = 0$ and $Q = 10$, as the Reynolds number is decreased across ST, the time-dependent 2-cell flow loses stability to the steady 2-cell flow. There is one exception to this for $Q = 0$ at the point S. Here, the curve takes a sharp upturn and the time-dependent 2-cell flow immediately loses stability to the steady 1-cell flow as ST is crossed (ST and CD do not actually meet). Further to the left of this point it is increasingly difficult to find the boundary of either CD or ST as the curves become nearly vertical. Because of this, any critical Reynolds numbers found are likely to be inaccurate. A similar situation arises for $Q = 10$ although it does not appear that the curve ST becomes too steep. To the left of the points D and S in both figures, a decrease of 0.01 in the aspect ratio does not allow the boundaries CD or ST to be extended further. Further calculations have shown the existence of the time-dependent 2-cell flow at $Q = 5$, but more work is necessary to explore the existence of this flow at other strengths of applied magnetic field and to better understand the transition boundaries for $Q = 0$ and $Q = 10$.

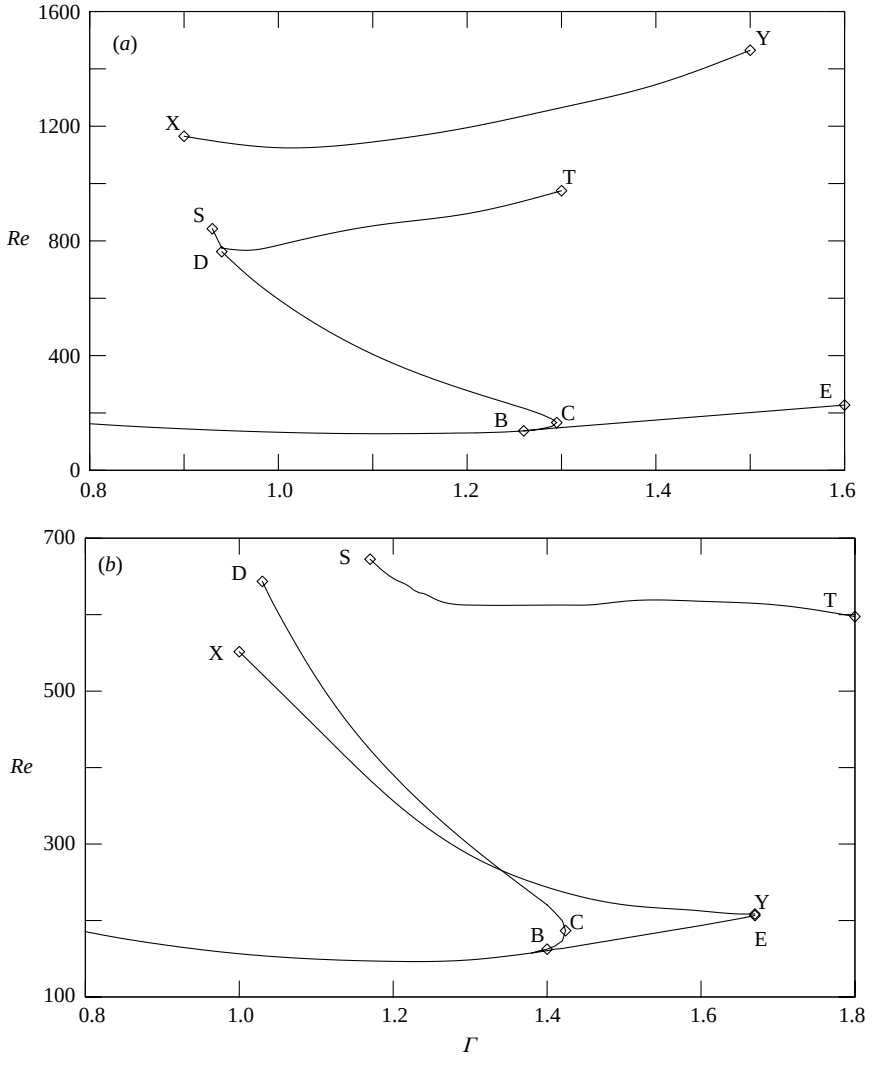

FIGURE 13. Reynolds number versus aspect ratio showing the boundary for the transition to the 2-cell time-dependent flow, for (*a*) $Q = 0$, (*b*) $Q = 10$.

5. Conclusion

In conclusion, the presence of a body force, such as an axially imposed magnetic field, does not reduce the multiplicity of solutions available even at small aspect ratio, which was revealed by Benjamin, Mullin, Pfister and others. However, if one increases the magnetic field, the general trend is that a larger Reynolds number is necessary to obtain steady 1-cell states, that is, steady 2-cell states are more stable. We have also found that, under an applied magnetic field, it is easy to excite time-dependent flows at relatively small Reynolds numbers. Hydromagnetic Couette flow seems to be a very rich system, and the work presented here is only an initial investigation of axisymmetric flows in a restricted region of parameter space. Further work will consider time-dependent 2-cell flows under a larger magnetic field, what happens at

smaller aspect ratio, the effect of electrically insulating boundary conditions and the possibility of non-axisymmetric motion.

A.J.Y. is grateful to Tom Mullin for discussions.

Appendix. Boundary conditions

Using cylindrical coordinates, the stream function ψ is defined by $u_r = -(1/r)\partial_z \psi$ and $u_z = (1/r)\partial_r \psi$.

From the no-slip boundary condition at the cylinder walls, $u_r = 0$ at $r = R_1$ and R_2, we find that $\partial_z \psi = 0$ at $r = R_1$ and R_2. Integrating and setting the arbitrary constant equal to zero we conclude that $\psi = 0$ at $r = R_1$ and R_2. Similarly, from the condition $u_z = 0$ at $z = 0$ and h we conclude that $\psi = 0$ at $z = 0$ and h.

Boundary conditions for the azimuthal vorticity ω_θ must be derived from those for ψ. The equation for the azimuthal vorticity is

$$\omega_\theta = -\frac{1}{r}\frac{\partial^2 \psi}{\partial z^2} - \frac{1}{r}\frac{\partial^2 \psi}{\partial r^2} + \frac{1}{r^2}\frac{\partial \psi}{\partial r}. \tag{A 1}$$

The first r- and second z-derivatives vanish at the cylinder walls due to the no-slip boundary conditions for u_z, and hence, $\omega_\theta = (-1/r)\partial_{rr}\psi$ at $r = R_1$ and R_2. Similarly, $\omega_\theta = (-1/r)\partial_{zz}\psi$ at $z = 0$ and h.

The electric field, $\boldsymbol{E}$ must be continuous at the cylinder walls, so $\hat{\boldsymbol{n}} \wedge (\boldsymbol{E}^c - \boldsymbol{E}^f) = 0$, where the superscripts c and f refer to the electric field in the cylinder and fluid respectively, and $\hat{\boldsymbol{n}}$ is the unit normal to a cylinder wall ($\hat{\boldsymbol{n}} = \pm \hat{\boldsymbol{r}}$).

In general, $\hat{\boldsymbol{r}} \wedge \boldsymbol{E} = (0, -E_z, E_\theta)$, so to match the electric field across the boundary we require $E_z^c = E_z^f$ and $E_\theta^c = E_\theta^f$. Using Ohm's law $\boldsymbol{J} = \sigma \boldsymbol{E}$, where $\boldsymbol{J}$ is the current and σ the electrical conductivity, we then have $(1/\sigma_c)J_z^c = (1/\sigma_f)J_z^f$ and $(1/\sigma_c)J_\theta^c = (1/\sigma_f)J_\theta^f$.

Assuming that the cylinders are perfectly conducting, we take $\sigma_c \to \infty$ and from the second equation we conclude that $J_\theta^f = 0$ at $r = R_1$ and R_2.

The boundary condition for the azimuthal magnetic field is obtained from the equation $\boldsymbol{J} = \nabla \wedge \boldsymbol{B}$; using $(1/\sigma_c)J_z^c = (1/\sigma_f)J_z^f$ with $\sigma_c \to \infty$ we have $(1/r)B_\theta^f + \partial_r B_\theta^f - (1/r)\partial_\theta B_r^f = 0$, where the superscript f has the same meaning as before; assuming axisymmetry we conclude that $(1/r)B_\theta^f + \partial_r B_\theta^f = 0$ at $r = R_1$ and R_2.

We again require the electric field to be continuous across the endwall boundaries $z = 0$ and h, hence taking $\hat{\boldsymbol{n}} = \pm \hat{\boldsymbol{z}}$ we have $\hat{\boldsymbol{z}} \wedge (\boldsymbol{E}^c - \boldsymbol{E}^f) = 0$.

Since, $\hat{\boldsymbol{z}} \wedge \boldsymbol{E} = (-E_\theta, E_r, 0)$, we have $E_\theta^c = E_\theta^f$ and $E_r^c = E_r^f$. As before, using Ohm's law we then have $(1/\sigma_c)J_\theta^c = (1/\sigma_f)J_\theta^f$ and $(1/\sigma_c)J_r^c = (1/\sigma_f)J_r^f$, and using $\sigma_c \to \infty$ we have that $J_\theta^f = 0$ at $z = 0$ and h.

Since $\boldsymbol{J} = \nabla \wedge \boldsymbol{B}$, from the first equation with $\sigma_c \to \infty$ we have $(1/r)\partial_\theta B_z^f - \partial_z B_\theta^f = 0$, and under the assumption of axisymmetry we conclude that $\partial_z B_\theta^f = 0$ at $z = 0$ and h.

REFERENCES

Benjamin, T. B. 1978*a* Bifurcation phenomena in steady flows of a viscous fluid. I. Theory. *Proc. R. Soc. Lond.* A **359**, 1–26.

Benjamin, T. B. 1978*b* Bifurcation phenomena in steady flows of a viscous fluid. II. Experiment. *Proc. R. Soc. Lond.* A **359**, 27–43.

Benjamin, T. B. & Mullin, T. 1981 Anomalous modes in the Taylor experiment. *Proc. R. Soc. Lond.* A **377**, 221–249.

Blackford, L. S., Choi, J., Cleary, A., D'Azevedo, E., Demme, J., Dhillon, I., Dongarra, J., Hammarling, S., Henry, G., Petitet, A., Stanley, K., Walker, D. & Whaley, R. C. 1997 *ScaLAPACK Users' Guide*. Philadelphia: Society for Industrial and Applied Mathematics.

Chandrasekhar, S. 1961 *Hydrodynamic and Hydromagnetic Stability*. Clarendon.

Cliffe, K. A. 1983 Numerical calculations of two-cell and single-cell Taylor flows. *J. Fluid Mech.* **135**, 219–233.

Cliffe, K. A., Kobine, J. J. & Mullin, T. 1992 The role of anomalous modes in Taylor–Couette flow. *Proc. R. Soc. Lond.* A **439**, 341–357.

Dobler, W., Shukurov, A. & Brandenburg, A. 2002 Nonlinear states of the screw dynamo. *Phys. Rev.* E **65**, 036311.

Donnelly, R. J. & Ozima, M. 1962 Experiments on the stability of flow between rotating cylinders in the presence of a magnetic field. *Proc. R. Soc. Lond.* A **226**, 272–286.

Furukawa, H., Watanabe, T., Toya, Y. & Nakamura, I. 2002 Flow pattern exchange in the Taylor–Couette system with a very small aspect ratio. *Phys. Rev.* E **65**, 036306.

Goodman, J. & Ji, H. T. 2002 Magnetorotational instability of dissipative Couette flow. *J. Fluid Mech.* **462**, 365–382.

Lensch, B. 1988 Über die dynamik der einwirbelströmung im Taylor-Zylinder. Diplomarbeit, University of Kiel, Germany.

Lopez, J. M. & Marques, F. 2003 Small aspect ratio Taylor–Couette flow: Onset of a very-low-frequency three-torus state. *Phys. Rev.* E **68**, 036302.

Lücke, M., Mihelcic, M., Wingerath, K. & Pfister, G. 1984 Flow in a small annulus between concentric cylinders. *J. Fluid Mech.* **140**, 343–353.

Mullin, T., Toya, Y. & Tavener, S. J. 2002 Symmetry breaking and multiplicity of states in small aspect ratio Taylor–Couette flow. *Phys. Fluids* **14**, 2778–2787.

Pfister, G., Schmidt, H., Cliffe, K. A. & Mullin, T. 1988 Bifurcation phenomena in Taylor–Couette flow in a very short annulus. *J. Fluid Mech.* **191**, 1–18.

Pfister, G., Schulz, A. & Lensch, B. 1991 Bifurcations and a route to chaos of a one-vortex-state in Taylor–Couette flow. *Eur. J. Mech.* B/*Fluids* **10**, 247–252.

Roberts, P. H. 1964 The stability of hydromagnetic Couette flow. *Proc. Camb. Phil. Soc.* **60**, 635–651.

Rüdiger, G., Schultz, M. & Shalybkov, D. 2003 Linear magnetohydrodynamic Taylor–Couette instability for liquid sodium. *Phys. Rev.* E **67**, 046312.

Schulz, A., Pfister, G. & Tavener, S. J. 2003 The effect of outer cylinder rotation on Taylor–Couette flow at small aspect ratio. *Phys. Fluids* **15**, 417–425.

Sisan, D. R., Mujica, N., Tillotson, W. A., Huang, Y. M., Dorland, W., Hassam, A. B., Antonsen, T. M. & Lathrop, D. P. 2004 Experimental observation and characterization of the magnetorotational instability. *Phys. Rev. Lett.* **93**, 114502.

Willis, A. P. & Barenghi, C. F. 2002*a* Magnetic instability in a sheared azimuthal flow. *Astron. Astrophys.* **388**, 688–691.

Willis, A. P. & Barenghi, C. F. 2002*b* A Taylor–Couette dynamo. *Astron. Astrophys.* **393**, 339–343.